

# Enhanced phase estimation in parity detection based Mach-Zehnder interferometer using non-Gaussian two-mode squeezed thermal input state

Chandan Kumar,<sup>1,\*</sup> Rishabh,<sup>2,†</sup> and Shikhar Arora<sup>1,‡</sup>

<sup>1</sup>*Department of Physical Sciences, Indian Institute of Science Education and Research Mohali, Sector 81 SAS Nagar, Punjab 140306 India.*

<sup>2</sup>*Department of Physics and Astronomy, University of Calgary, Calgary T2N1N4, Alberta, Canada.*

While the quantum metrological advantages of performing non-Gaussian operations on two-mode squeezed vacuum (TMSV) states have been extensively explored, similar studies in the context of two-mode squeezed thermal (TMST) states are severely lacking. In this paper, we explore the potential advantages of performing non-Gaussian operations on TMST state for phase estimation using parity detection based Mach-Zehnder interferometry. To this end, we consider the realistic model of photon subtraction, addition, and catalysis. We first provide a derivation of the unified Wigner function of the photon subtracted, photon added and photon catalyzed TMST state, which to the best of our knowledge is not available in the existing literature. This Wigner function is then used to obtain the expression for the phase sensitivity. Our results show that performing non-Gaussian operations on TMST states can enhance the phase sensitivity for significant ranges of squeezing and transmissivity parameters. We also observe that incremental advantage provided by performing these non-Gaussian operations on the TMST state is considerably higher than that of performing these operations on the TMSV state. Because of the probabilistic nature of these operations, it is of utmost importance to take their success probability into account. We identify the photon catalysis operation performed using a high transmissivity beam splitter as the optimal non-Gaussian operation when the success probability is taken into account. This is in contrast to the TMSV case, where we observe photon addition to be the most optimal. These results will be of high relevance for any future phase estimation experiments involving TMST states. Further, the derived Wigner function of the non-Gaussian TMST states will be useful for state characterization and its application in various quantum information protocols.

## I. INTRODUCTION

Optical interferometers have played an important role in the advancement of quantum sensing [1, 2]. In particular, Mach-Zehnder interferometer (MZI) has been extensively utilized for phase sensitivity studies. While the phase sensitivity of MZI using classical resources is limited by so called shot-noise limit (SNL) [3], quantum resources, such as, squeezed states and entangled states can break the SNL and achieve the Heisenberg limit (HL) [4–7]. Many quantum states of light have been employed in parity measurement based optical interferometry to reach HL with the notable example of N00N states [6, 8–20]. However, photon loss renders N00N states fragile to environmental interactions. Moreover, it has been shown that two-mode squeezed vacuum (TMSV) states can even break the HL limit [6], but their implementation is limited by the maximum achievable squeezing [21].

To overcome the hindrance caused by the upper limit on the maximum achievable squeezing, one can resort to the engineering of non-Gaussian states by performing photon subtraction (PS), photon addition (PA), or photon catalysis (PC) operations on the TMSV state. These non-Gaussian states have enhanced squeezing and entanglement, which have been utilised for performance im-

provement in quantum key distribution [22–27], quantum teleportation [28–32] as well as quantum metrology [33–38].

Thermal states are an important class of mixed Gaussian states, which have played a key role in quantum optics from its inception [39]. These states have since then been used in various practical applications, such as, thermal lasers [40], ghost imaging [41–43], and quantum illumination [44]. Two-mode squeezed thermal (TMST) state have been proposed for use in quantum phase estimation [45]. TMST states have also been realized experimentally [46–49]. Further, non-Gaussian operations on squeezed thermal states are also being considered actively. For instance, nonclassicality and entanglement have been explored in photon subtracted and added squeezed thermal states [50–53]. Similarly, photon subtracted TMST (PSTMST) and photon added TMST (PATMST) states have also been proposed as resources for quantum teleportation [54]. There have been experimental efforts in the preparation, reconstruction and statistical parameter estimation of multiphoton subtracted thermal states [55, 56].

Motivated by these studies, we aim to determine whether non-Gaussian operations such as PS, PA and PC can improve the phase sensitivity of the original TMST state. To this end, we consider the experimental model of PS, PA and PC operations [57] (see Fig.1). Next, we obtain the Wigner function describing the PSTMST, PATMST and photon catalyzed TMST (PCTMST) states, which is utilized to evaluate the phase

\* chandan.quantum@gmail.com

† rishabh1@ucalgary.ca

‡ shikhar.quantum@gmail.com

sensitivity of the parity detection based MZI. In this paper, we will collectively refer PSTMST, PATMST, and PCTMST states as NGTMST states, where “NG” stands for non-Gaussian. Also note that from here on, the term non-Gaussian operations will be used only to refer PA, PS, and PC operations unless stated otherwise.

We emphasize that the presence of an additional parameter in the TMST state (average number of photons in the thermal state) significantly enhances the complexity of analytical calculations of the involved quantities as compared to TMSV state. We employ the phase space formalism rather than the more often used operator formalism because of the computational ease provided by the former [58].

Our results clearly demonstrate that the non-Gaussian operations can significantly enhance a TMST state’s phase sensitivity. To better understand the above results and to find out the squeezing and transmissivity values rendering an enhancement in phase sensitivity using NGTMST resource states, we have shown the plots for the difference between the phase sensitivity of the TMST and NGTMST states in squeezing-transmissivity plane. Further, with a view to identify optimal non-Gaussian operations, we take the probabilistic nature of non-Gaussian operations into our consideration. A careful analysis shows that only for photon catalysis, the parameter values corresponding to large enhancement overlap with those corresponding to a region of high success probability, which happens in a large transmissivity regime. Hence, it can be concluded that of all non-Gaussian operations, implementing PC using a high transmissivity beam splitter is the optimal choice. This is contrary to the case involving non-Gaussian TMSV state, where PA operation comes out to be most optimal [38].

Also, the expression for unified Wigner function of NGTMST states derived here, do not appear in the existing literature to the best of our knowledge. This expression will be a welcome addition to existing literature and will find important use while dealing with various CV QIP protocols involving NGTMST states. Additionally, we supply a single expression for the parity detection-based phase sensitivity to deal with all three non-Gaussian operations performed on the TMST state at once.

The layout of this paper is as follows. In Sec. II, we present a brief overview of the formalism for CV systems. In Sec. III, we derive the unified Wigner function for all the NGTMST states. Section IV contains a short description of parity-detection based lossless MZI. We start by comparing the phase sensitivities of the TMSV and TMST states. We then show the advantages of using NGTMST states over TMST states to determine the phase for specific chosen values of involved parameters. Next, we move on to a more involved analysis by studying the difference between the phase sensitivity of the TMST and NGTMST states and the success probability of corresponding non-Gaussian operations for experimentally reasonable values of squeezing and transmissivity. To

gain a better perspective, we also compare our results to the case of non-Gaussian TMSV state (Ref [38]). Finally, in Sec. V, we conclude the article by summarizing the main points and discussing possible future directions.

## II. BRIEF DESCRIPTION OF CV SYSTEMS

We consider an  $n$ -mode quantum optical system, whose  $i^{\text{th}}$  mode can be represented by a pair of Hermitian quadrature operators  $\hat{q}_i$  and  $\hat{p}_i$ . For convenience, we define the following  $2n$ -dimensional column vector comprising of  $n$  pairs of Hermitian quadrature operators:

$$\hat{\xi} = (\hat{\xi}_i) = (\hat{q}_1, \hat{p}_1, \dots, \hat{q}_n, \hat{p}_n)^T, \quad i = 1, 2, \dots, 2n. \quad (1)$$

In terms of the column vector  $\hat{\xi}$ , the canonical commutation relation can be formulated as

$$[\hat{\xi}_i, \hat{\xi}_j] = i\Omega_{ij}, \quad (i, j = 1, 2, \dots, 2n), \quad (2)$$

where we have taken  $\hbar=1$ , and  $\Omega$  is a  $2n \times 2n$  matrix given by

$$\Omega = \bigoplus_{k=1}^n \omega = \begin{pmatrix} \omega & & \\ & \ddots & \\ & & \omega \end{pmatrix}, \quad \omega = \begin{pmatrix} 0 & 1 \\ -1 & 0 \end{pmatrix}. \quad (3)$$

The photon annihilation and creation operators for the  $i^{\text{th}}$  mode are defined in terms of the corresponding quadrature operators as follows:

$$\hat{a}_i = \frac{1}{\sqrt{2}}(\hat{q}_i + i\hat{p}_i), \quad \hat{a}_i^\dagger = \frac{1}{\sqrt{2}}(\hat{q}_i - i\hat{p}_i). \quad (4)$$

For a quantum system with density operator  $\hat{\rho}$ , we can define the Wigner distribution function as below:

$$W(\boldsymbol{\xi}) = \int \frac{d^n \mathbf{q}'}{(2\pi)^n} \left\langle \mathbf{q} - \frac{1}{2}\mathbf{q}' \left| \hat{\rho} \left| \mathbf{q} + \frac{1}{2}\mathbf{q}' \right. \right. \right\rangle \exp(i\mathbf{q}'^T \cdot \mathbf{p}), \quad (5)$$

where  $\boldsymbol{\xi} = (q_1, p_1, \dots, q_n, p_n)^T \in \mathbb{R}^{2n}$ ,  $\mathbf{q}' \in \mathbb{R}^n$  and  $\mathbf{q} = (q_1, q_2, \dots, q_n)^T$ ,  $\mathbf{p} = (p_1, p_2, \dots, p_n)^T$ . The Wigner function of a Fock state  $|n\rangle$  can be evaluated using Eq. (5) as

$$W_{|n\rangle}(q, p) = \frac{(-1)^n}{\pi} \exp(-q^2 - p^2) L_n[2(q^2 + p^2)], \quad (6)$$

where  $L_n\{\bullet\}$  is the Laguerre polynomial of  $n$ th order. We can also reformulate the Wigner function in terms of the average of displaced parity operator [59]:

$$W(\boldsymbol{\xi}) = \frac{1}{\pi^n} \text{Tr} \left[ \hat{\rho} D(\boldsymbol{\xi}) \hat{\Pi} D^\dagger(\boldsymbol{\xi}) \right], \quad (7)$$

where  $\hat{\Pi} = \prod_{i=0}^n \exp(i\pi \hat{a}_i^\dagger \hat{a}_i)$  is the parity operator and  $D(\boldsymbol{\xi}) = \exp[i\hat{\xi}^T \Omega \boldsymbol{\xi}]$  is the displacement operator.

Gaussian states are an important class of CV-system states whose Wigner distribution is a Gaussian function.

The Wigner function (5) for  $n$ -mode Gaussian states simplifies to the following form [60]:

$$W(\xi) = \frac{\exp[-(1/2)(\xi - \mathbf{d})^T V^{-1}(\xi - \mathbf{d})]}{(2\pi)^n \sqrt{\det V}}, \quad (8)$$

where  $\mathbf{d} = \text{Tr}[\hat{\rho}\hat{\xi}]$  is the displacement vector and  $V$  is a  $2n \times 2n$  covariance matrix, whose element can be calculated as

$$V_{ij} = \frac{1}{2} \langle \{ \Delta \hat{\xi}_i, \Delta \hat{\xi}_j \} \rangle, \quad (9)$$

where  $\Delta \hat{\xi}_i = \hat{\xi}_i - \langle \hat{\xi}_i \rangle$ , and  $\{, \}$  denotes anti-commutator. The action of an infinite-dimensional unitary operator  $\mathcal{U}$  on a density operator can be mapped to a symplectic transformation  $S \in Sp(2n, \mathcal{R})$  acting on the quadrature operators. Further, the state evolution  $\rho \rightarrow \mathcal{U}\rho\mathcal{U}^\dagger$  can be rephrased as a symplectic transformation in phase space as follows [61]:

$$\mathbf{d} \rightarrow S\mathbf{d}, \quad V \rightarrow SVS^T, \quad \text{and } W(\xi) \rightarrow W(S^{-1}\xi). \quad (10)$$

Quantum optical mode in thermal equilibrium with a bath at a given temperature is said to be in a thermal state. This mode can be thought of as a classical mixture of different photon number states with weight factors given by the Boltzmann distribution. As stated earlier in this paper, we consider the TMST state, which can be generated by subjecting two uncorrelated thermal modes to a two mode squeezing transformation. The TMST state is described by the following covariance matrix:

$$V_{A_1 A_2} = S_{A_1 A_2}(r) V_{\text{th}} S_{A_1 A_2}(r)^T, \quad (11)$$

where  $V_{\text{th}} = (n_{\text{th}} + 1/2)\mathbb{1}_4$  is the covariance matrix of the two uncorrelated thermal modes with  $n_{\text{th}}$  being the average number of photons in the thermal state. Further,  $S_{A_1 A_2}(r)$  is the two mode squeezing transformation given by

$$S_{A_1 A_2}(r) = \begin{pmatrix} \cosh r \mathbb{1}_2 & \sinh r \mathbb{Z} \\ \sinh r \mathbb{Z} & \cosh r \mathbb{1}_2 \end{pmatrix}, \quad \mathbb{Z} = \begin{pmatrix} 1 & 0 \\ 0 & -1 \end{pmatrix}. \quad (12)$$

Putting  $n_{\text{th}} = 0$  in Eq. (12), we obtain the covariance matrix of the TMSV state. Since TMST state is a Gaussian state with zero mean and covariance matrix given by Eq. (12), the Wigner function of the TMST state can be readily evaluated using Eq. (8):

$$W(\xi) = \frac{1}{(2\pi\kappa)^2} \exp \left[ - (q_1^2 + p_1^2 + q_2^2 + p_2^2) \cosh(2r)/(2\kappa) + (q_1 q_2 - p_1 p_2) \sinh(2r)/\kappa \right], \quad (13)$$

where  $\kappa = (n_{\text{th}} + 1/2)$ . We now discuss PS, PA, and PC operations on a TMST state.

### III. WIGNER FUNCTION OF NGTMST STATES

The schematic for the generation of NGTMST states is shown in Fig. 1. Mode  $A_2$  of the TMST state is mixed

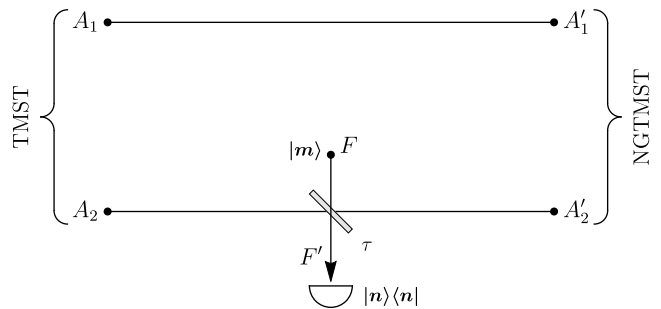


FIG. 1. Schematic for the preparation of NGTMST states. The mode  $A_2$  of the TMST state is mixed with Fock state  $|m\rangle$  using a beam splitter of transmissivity  $\tau$ . Photon number measurement is performed on the output auxiliary mode to obtain the NGTMST states.

with auxiliary mode  $F$ , which is in Fock state  $|m\rangle$ , via beam-splitter of transmissivity  $\tau$ . We represent the state of the three mode system before the beam splitter operation via its Wigner function:

$$W_{A_1 A_2 F}(\xi) = W_{A_1 A_2}(\xi_1, \xi_2) W_{|m\rangle}(\xi_3), \quad (14)$$

where  $\xi_i = (q_i, p_i)^T$  ( $i = 1, 2, 3$ ). The beam-splitter transforms the phase space variables  $(\xi_2, \xi_3)^T$  via the symplectic transformation

$$B_{A_2 F}(\tau) = \begin{pmatrix} \sqrt{\tau} \mathbb{1}_2 & \sqrt{1-\tau} \mathbb{1}_2 \\ -\sqrt{1-\tau} \mathbb{1}_2 & \sqrt{\tau} \mathbb{1}_2 \end{pmatrix}. \quad (15)$$

The Wigner function after the beam-splitters operation is given by

$$W_{A_1' A_2' F'}(\xi) = W_{A_1 A_2 F}([\mathbb{1}_2 \oplus B_{A_2 F}(\tau)]^{-1}\xi). \quad (16)$$

A photon number resolving detector, represented by the positive-operator-valued measure (POVM)  $\{\Pi_n = |n\rangle\langle n|, \mathbb{1} - \Pi_n\}$  is employed to measure the mode  $F'$ . When the POVM element  $\Pi_n$  clicks, the non-Gaussian operation is performed successfully on the mode  $A_2$ . The expression for corresponding probability is provided in Eq. (23). The reduced state is NGTMST states, and its unnormalized Wigner function is given by

$$\widetilde{W}_{A_1' A_2'}^{\text{NG}}(\xi_1, \xi_2) = 2\pi \int d^2 \xi_3 \underbrace{W_{A_1' A_2' F'}(\xi_1, \xi_2, \xi_3)}_{\text{Three mode entangled state}} \times \underbrace{W_{|n\rangle}(\xi_3)}_{\text{Projection on } |n\rangle\langle n|}. \quad (17)$$

By carefully selecting the values of the parameters  $(m, n)$ , we can perform the required non-Gaussian operations. For PS operation,  $m < n$ , whereas for PA operation,  $m > n$ . Lastly, for PC operation,  $m = n$ . PS operation on TMST states yields PSTMST states. Similarly, PA and PC operations on TMST states yields PATMST and PCTMST states, respectively.

The generating function for the Laguerre polynomials

$$L_n[2(q^2 + p^2)] = \widehat{D} \exp \left[ \frac{st}{2} + s(q + ip) - t(q - ip) \right], \quad (18)$$

with

$$\widehat{D} = \frac{2^n}{n!} \frac{\partial^n}{\partial s^n} \frac{\partial^n}{\partial t^n} \{\bullet\}_{s=t=0}. \quad (19)$$

can be used to convert Eq. (17) into a Gaussian integral. On integration of Eq. (17), we get

$$\begin{aligned} \widetilde{W}_{A'_1 A'_2}^{\text{NG}} &= \frac{\exp(\boldsymbol{\xi}^T M_1 \boldsymbol{\xi})}{a_0} \widehat{D}_1 \exp \left[ -a_1 u_1 v_1 + a_2 u_1 + a_3 v_1 \right. \\ &\quad \left. - a_4 u_2 v_2 + a_5 u_2 + a_6 v_2 + a_7(u_1 u_2 + v_1 v_2) \right], \end{aligned} \quad (20)$$

where the column vector  $\boldsymbol{\xi}$  is defined as  $(q_1, p_1, q_2, p_2)^T$  and the coefficients  $a_i$  and the matrix  $M_1$  are defined in Eqs. (A1) and (A3) of the Appendix A, respectively. Further, the differential operator  $\widehat{D}_1$  is given as

$$\widehat{D}_1 = \frac{(-2)^{m+n}}{m! n!} \frac{\partial^m}{\partial u_1^m} \frac{\partial^m}{\partial v_1^m} \frac{\partial^n}{\partial u_2^n} \frac{\partial^n}{\partial v_2^n} \{\bullet\}_{u_1=v_1=0, u_2=v_2=0}. \quad (21)$$

We can express Eq. (20) in terms of two-variable Hermite polynomials  $H_{m,n}(x, y)$ :

$$\begin{aligned} \widetilde{W}_{A'_1 A'_2}^{\text{NG}} &= \frac{(-2)^{m+n}}{m! n!} \frac{\exp(\boldsymbol{\xi}^T M_1 \boldsymbol{\xi})}{a_0} \sum_{i,j=0}^{\min(m,n)} \frac{a_1^m}{\sqrt{a_1}^{i+j}} \\ &\quad \times \frac{a_4^n}{\sqrt{a_4}^{i+j}} \frac{a_7^{i+j}}{i! j!} \frac{m!}{(m-i)!} \frac{m!}{(m-j)!} \frac{n!}{(n-i)!} \frac{n!}{(n-j)!} \\ &\quad \times H_{m-i, m-j} \left[ \frac{a_2}{\sqrt{a_1}}, \frac{a_3}{\sqrt{a_1}} \right] H_{n-i, n-j} \left[ \frac{a_5}{\sqrt{a_4}}, \frac{a_6}{\sqrt{a_4}} \right]. \end{aligned} \quad (22)$$

The probability of a successful non-Gaussian operation can be evaluated as

$$P^{\text{NG}} = \int d^2 \xi_1 d^2 \xi_2 \widetilde{W}_{A'_1 A'_2}^{\text{NG}} = d_0 \widehat{D}_1 \exp(\mathbf{u}^T M_2 \mathbf{u}), \quad (23)$$

where the column vector  $\mathbf{u}$  is defined as  $(u_1, v_1, u_2, v_2)^T$  and the matrix  $M_2$  and coefficient  $d_0$  are defined in Eqs. (A5) and (A6) of the Appendix A. The normalized Wigner characteristic function  $\widetilde{W}_{A'_1 A'_2}^{\text{NG}}$  of the non-Gaussian NGTMST state is obtained as

$$W_{A'_1 A'_2}^{\text{NG}}(\xi_1, \xi_2) = (P^{\text{NG}})^{-1} \widetilde{W}_{A'_1 A'_2}^{\text{NG}}(\xi_1, \xi_2). \quad (24)$$

The Wigner function of several special cases can be readily derived from Eq. (24). For example, in the unit transmissivity limit  $\tau \rightarrow 1$  with  $m = 0$ , we obtain the Wigner function of the ideal PSTMST state  $\mathcal{N}_s \hat{a}_2^n |\text{TMST}\rangle$  with  $\mathcal{N}_s$  being the normalization factor. Similarly, in the unit transmissivity limit  $\tau \rightarrow 1$  with  $n = 0$ , we obtain the Wigner function of the ideal PATMST state  $\mathcal{N}_a \hat{a}_2^{\dagger m} |\text{TMST}\rangle$  with  $\mathcal{N}_a$  being the normalization factor. Further, setting  $\kappa = 1/2$  (equivalently  $n_{\text{th}} = 0$ ) in Eq. (24) yields the Wigner function of the non-Gaussian TMSV state.

#### IV. PARITY DETECTION BASED PHASE SENSITIVITY IN MZI

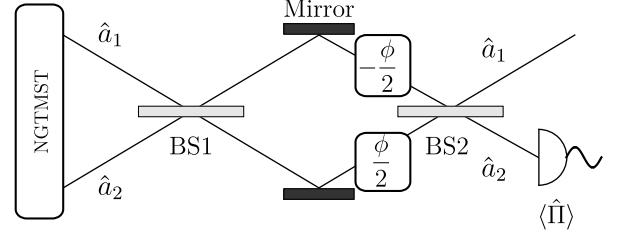


FIG. 2. Schematic of parity detection based Mach-Zehnder interferometer for detection of an unknown phase shift using NGTMST state as an input.

We consider a lossless MZI comprised of two 50:50 beam splitters and two phase shifters, as shown in Fig. 2. The NGTMST states are introduced as input in the interferometer. The annihilation operators  $\hat{a}_1$  and  $\hat{a}_2$  represent the two input modes. This setup is used for estimating the unknown phase  $\phi$  introduced via the two phase shifters by measuring the parity operator on the output mode  $\hat{a}_2$ .

To describe the mode transformations induced by the optical elements in the MZI, it is convenient to use the Schwinger representation of SU(2) algebra [62]. The generators of the SU(2) algebra, also known as angular momentum operators can be written in terms of the annihilation and creation operators of the input modes as follows:

$$\begin{aligned} \hat{J}_1 &= \frac{1}{2} (\hat{a}_1^\dagger \hat{a}_2 + \hat{a}_1 \hat{a}_2^\dagger), \\ \hat{J}_2 &= \frac{1}{2i} (\hat{a}_1^\dagger \hat{a}_2 - \hat{a}_1 \hat{a}_2^\dagger), \\ \hat{J}_3 &= \frac{1}{2} (\hat{a}_1^\dagger \hat{a}_1 - \hat{a}_2^\dagger \hat{a}_2). \end{aligned} \quad (25)$$

These angular momentum operators follow the commutation relations  $[J_i, J_j] = i\epsilon_{ijk} J_k$ . The infinite-dimensional unitary transformations of the first and the second beam splitters are given by  $e^{-i(\pi/2)J_1}$  and  $e^{i(\pi/2)J_1}$ , respectively. Further, the cumulative action of the two phase shifters is given by  $e^{i\phi J_3}$ . Hence, the overall action of the lossless MZI is given by

$$\mathcal{U}(S_{\text{MZI}}) = e^{-i(\pi/2)J_1} e^{i\phi J_3} e^{i(\pi/2)J_1} = e^{-i\phi J_2}. \quad (26)$$

The resultant symplectic transformation  $S_{\text{MZI}}$  of the MZI acting on the phase space variables  $(\xi_1, \xi_2)^T$  is given by

$$S_{\text{MZI}} = \begin{pmatrix} \cos(\phi/2) \mathbb{1} & -\sin(\phi/2) \mathbb{1} \\ \sin(\phi/2) \mathbb{1} & \cos(\phi/2) \mathbb{1} \end{pmatrix}. \quad (27)$$

The transformation of the Wigner function of the input state due to the MZI can be written using Eq. (10) as

$$W_{\text{in}}(\xi) \rightarrow W_{\text{in}}(S_{\text{MZI}}^{-1} \xi) = W_{\text{out}}(\xi). \quad (28)$$

As shown in the schematic of MZI (Fig. 2), we perform parity measurement on the output mode  $\hat{a}_2$ , which basically differentiates between even and odd photons numbers Fock state. The corresponding photon number parity operator is written as

$$\hat{\Pi}_{\hat{a}_2} = \exp\left(i\pi\hat{a}_2^\dagger\hat{a}_2\right) = (-1)^{\hat{a}_2^\dagger\hat{a}_2}. \quad (29)$$

Therefore, the average value of the parity measurement operator can be evaluated using Eq. (7) [63]:

$$\langle\hat{\Pi}_{\hat{a}_2}\rangle = f(\phi) = \pi \int d^2\xi_1 W_{\text{out}}(\xi_1, 0). \quad (30)$$

Using the Wigner function of the NGTMST state (24), the average of the parity measurement operator comes out to be

$$f(\phi) = \frac{e_0\hat{D}_1 \exp(\mathbf{u}^T M_3 \mathbf{u})}{d_0\hat{D}_1 \exp(\mathbf{u}^T M_2 \mathbf{u})}, \quad (31)$$

where the matrix  $M_3$  and coefficient  $e_0$  are defined in Eqs. (A7) and (A8) of the Appendix A. Taking the unit transmissivity limit under the condition  $m = n$  in Eq. (31), yields the average of the parity operator for the case of input TMST state:

$$f(\phi)_{\text{TMST}} = \frac{1 - \lambda^2}{2\kappa[1 + \lambda^4 - 2\lambda^2 \cos(2\phi)]^{1/2}}. \quad (32)$$

Further, setting  $\kappa = 1/2$  in Eq. (32) renders the average of the parity operator for an input TMSV state.

The error propagation formula allows us to write the phase uncertainty or sensitivity as

$$\Delta\phi = \frac{\sqrt{1 - f(\phi + \pi/2)^2}}{|\partial f(\phi + \pi/2)/\partial\phi|}. \quad (33)$$

The phase uncertainty for the input TMST state can be written using Eq. (32) as

$$\Delta\phi_{\text{TMST}} = \frac{\sqrt{\kappa^2 - \frac{(1 - \lambda^2)^2}{1 + \lambda^4 - 2\lambda^2 \cos(2\phi)}}}{\left|\frac{\lambda^2(1 - \lambda^2) \sin(2\phi)}{[1 + \lambda^4 - 2\lambda^2 \cos(2\phi)]^{3/2}}\right|}. \quad (34)$$

We note that the phase uncertainty depends on the following parameters:

- (i) Squeezing of the TMST state, referred to as squeezing from here on.
- (ii) Transmissivity of the beam splitter used in the implementation of the non-Gaussian operations, referred to as transmissivity from now onward.
- (iii) Magnitude of unknown phase introduced, which will be referred to as phase.
- (iv) Average number of photons in the thermal state.

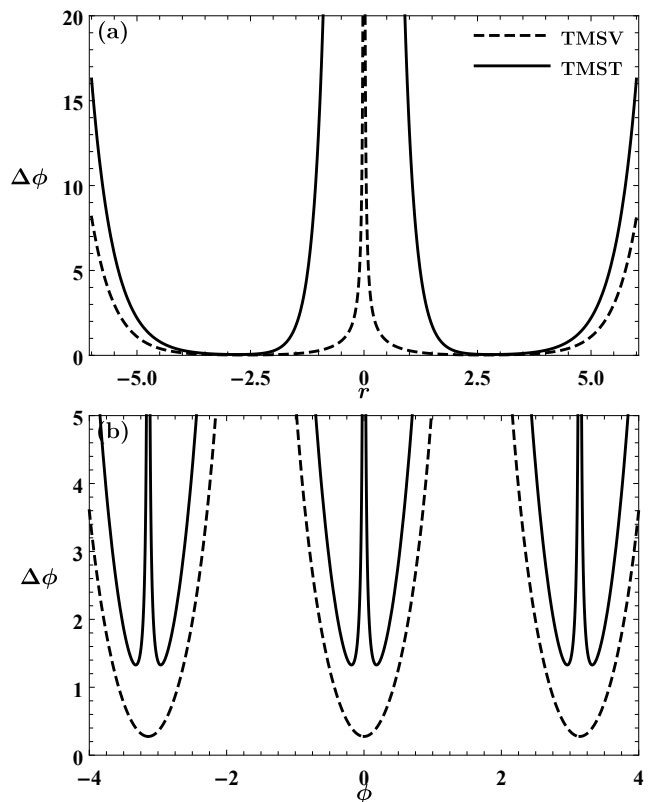


FIG. 3. (a) Phase uncertainty  $\Delta\phi$  as a function of squeezing parameter  $r$  for the TMST and TMSV states. We have taken  $\phi = 0.01$  rad. (b) Phase uncertainty  $\Delta\phi$  as a function of phase  $\phi$ . We have taken  $r = 1$ . Further, we have set  $\kappa = 1$  for the TMST state for both the panels. While  $\Delta\phi$  and  $\phi$  axes are in rad,  $r$  axis is dimensionless.

We now numerically study the dependence of the phase uncertainty of the input TMSV and TMST states on squeezing and phase (the thermal parameter  $\kappa$  has been set equal to 1 for TMST state throughout the article). The results are shown in Fig. 3. As is evident from Eq. (34), the phase uncertainty for the input TMST state will be larger than the input TMSV state, which can also be seen in Fig. 3. As is shown in Fig. 3(a), the phase uncertainty blows up at  $r = 0$  for both the TMSV and TMST states and attains a minima at  $r \approx 2.65$  and  $r \approx 2.80$ , respectively. However, such large values of squeezing cannot be achieved with current technology [21]. We note here that these specific numerical values of squeezing are for  $\phi = 0.01$ .

As is obvious from Eq. (34), the phase uncertainty varies periodically with period  $\pi$  as a function of phase, which can also be seen in Fig. 3(b). The phase uncertainty for the TMSV state is minimized at  $\phi = 0, \pm\pi, \pm2\pi, \dots$ , whereas for the TMST state, it blows up at these values with a pair of minima appearing in the surrounding regions.

### A. Advantages of non-Gaussian operations on TMST state in phase estimation

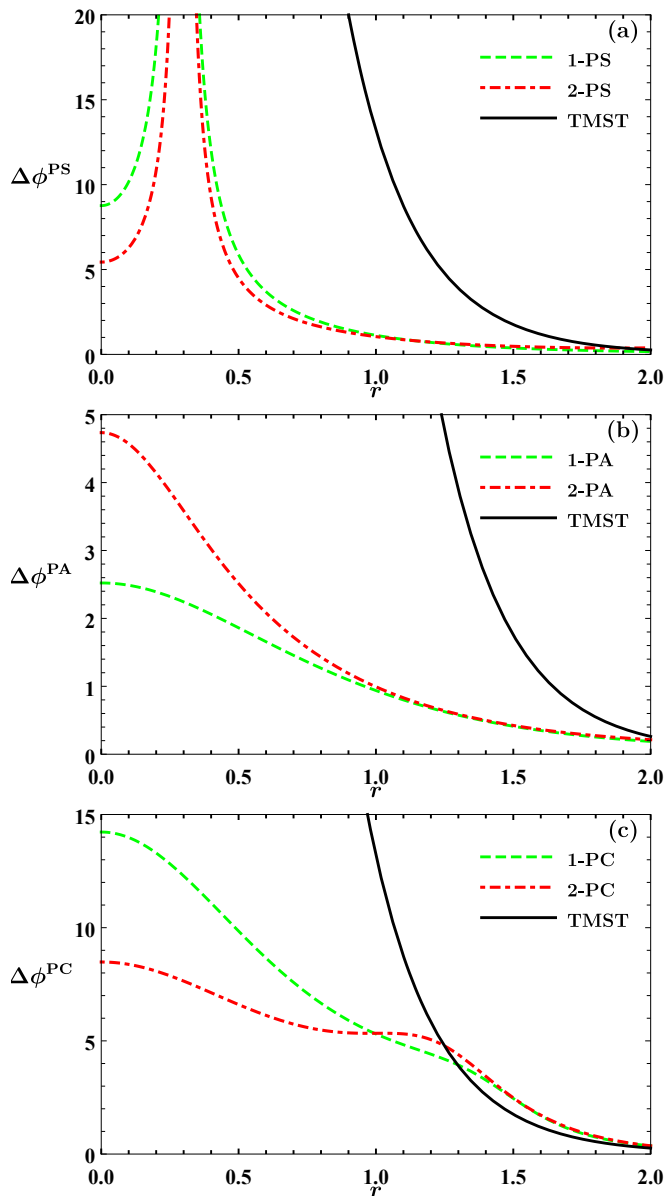


FIG. 4. Phase uncertainty  $\Delta\phi$  as a function of the squeezing parameter  $r$  for TMST and various NGTMST states. We have set the  $\tau = 0.9$  and  $\phi = 0.01$  rad for all the panels. While  $\Delta\phi$  axis is in rad,  $r$  axis is dimensionless.

In this section, we explore the advantages of performing the non-Gaussian operations on TMST state in the context of phase estimation. As we shall see, various NGTMST states outperform the original TMST state. We first analyze the dependency of the phase uncertainty on initial squeezing ( $r$ ) while transmissivity ( $\tau$ ), and magnitude of phase ( $\phi$ ) are kept fixed at suitably chosen values (see Fig. 4). In Fig. 4(a), we observe that 1-PSTMST and 2-PSTMST states improve the phase sen-

sitivity over the original TMST states. It is also interesting to note that the value of  $\Delta\phi^{\text{PS}}$  blows up at  $r \approx 0.3$ . Similar features can also be observed for other NGTMST states if parameter values are appropriately chosen. As seen in Fig. 4(b), both the 1-PATMST and 2-PATMST states outperform the original TMST state. We also notice that for upto  $r \approx 1$ , 1-PATMST state outperforms 2-PATMST state, which is in contrast with Fig. 4(a), where 2-PSTMST state outperforms 1-PSTMST state. Figure 4(c) shows that 1-PCTMST and 2-PCTMST states outperform the TMST state up to  $r \approx 1.3$ . While 1-PCTMST state performs better for  $r \lesssim 1.0$ , it is outperformed by 2-PCTMST state beyond this squeezing.

In Fig. 5, we show the phase uncertainty with respect to transmissivity at a given squeezing and phase value. It can be clearly seen that for given values of squeezing and phase, all NGTMST states outperform the TMST state for all transmissivity values. We also notice that the phase sensitivity improves with increasing  $\tau$  for PSTMST and PATMST states. Moreover, as we can see in Fig. 5(c), either the 1-PCTMST or 2-PCTMST states can provide better phase sensitivity depending on the value of transmissivity. Also, the phase uncertainty of the PCTMST states approaches that of the TMST state in the unit transmissivity limit.

In Fig. 6, we plot the phase uncertainty with respect to phase magnitude at a given squeezing and transmissivity values. While PSTMST and PATMST states improve the phase sensitivity for small phase values, PCTMST states can enhance the phase sensitivity even for larger phase values.

### B. Success probability and relative performances of NGTMST states in phase estimation

In the previous section, we explored the advantages of using NGTMST states over the original TMST state for certain specifically chosen values of state parameters ( $r$  and  $\tau$ ) and phase  $\phi$ . In order to gain a comprehensive insight into the comparative performances of NGTMST and TMST states in the context of phase estimation, we now explore the advantages of using non-Gaussian resources for a reasonable range of transmissivity and squeezing parameters for a given value of phase. For this purpose, we start by defining a figure of merit,  $\mathcal{D}_T^{\text{NG}}$ , as the difference of  $\Delta\phi$  between TMST and NGTMST states:

$$\mathcal{D}_T^{\text{NG}} = \Delta\phi^{\text{TMST}} - \Delta\phi^{\text{NGTMST}}, \quad (35)$$

where the subscript  $T$  stands for thermal in the TMST state. The region of positive  $\mathcal{D}_T^{\text{NG}}$  corresponds to those values of transmissivity and squeezing for which the NGTMST states perform better than the TMST state.

To better understand the impact of the probabilistic nature of non-Gaussian operations, we plot the success probability alongside the  $\mathcal{D}_T^{\text{NG}}$  for the same state parameter ranges. Success probability is also a good measure

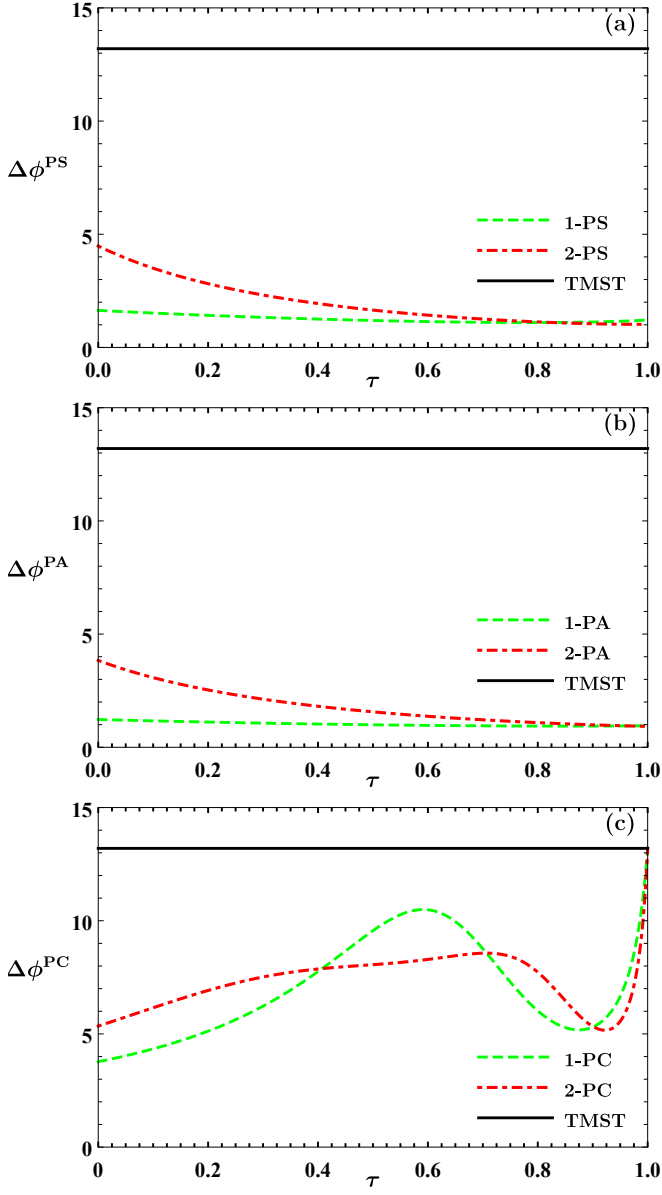


FIG. 5. Phase uncertainty  $\Delta\phi$  as a function of the transmissivity  $\tau$  for TMST and various NGTMSV states. We have set the squeezing as  $r = 1$  for all the panels. Further, we have taken  $\phi = 0.01$  rad in all the panels. While  $\Delta\phi$  axis is in rad,  $\tau$  axis is dimensionless.

of resource utilization and can be defined as the fraction of successful non-Gaussian operations.

For comparative purposes, we reproduce the results of Ref. [38] in Fig. 7, which demonstrates the advantages of performing non-Gaussian operations on the TMSV state in the context of phase estimation. The equivalent figure of merit (35) for NGTMSV states can be written as

$$\mathcal{D}_V^{\text{NG}} = \Delta\phi^{\text{TMSV}} - \Delta\phi^{\text{NGTMSV}}, \quad (36)$$

where the subscript  $V$  stands for vacuum in the TMSV state. In the left panels of Fig. 7, success probability

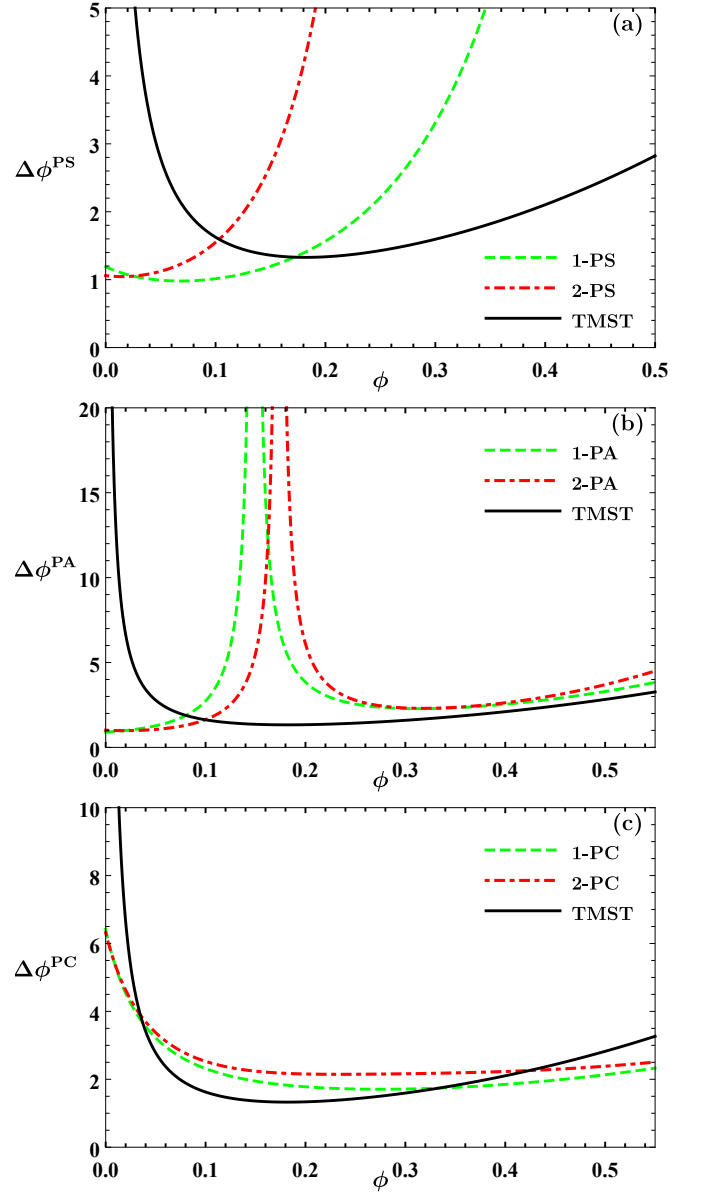


FIG. 6. Phase uncertainty  $\Delta\phi$  as a function of the phase  $\phi$  for TMST and various NGTMSV states. We have set the  $\tau = 0.9$  and  $r = 1$  for all the panels. Both  $\Delta\phi$  and  $\phi$  axes are in rad.

for various non-Gaussian operations are plotted, whereas the right panels show the plot for different fixed values of corresponding  $\mathcal{D}_V^{\text{NG}}$  ( $= 0.0, 0.1, 0.5, 1, 2, 3$ ) as a function of the transmissivity  $\tau$  and squeezing parameter  $r$ . Positive  $\mathcal{D}_V^{\text{NG}}$  corresponds to that region in the  $(\tau, r)$  space where the NGTMSV states outperform the TMSV state. A careful comparison of different non-Gaussian operations shows that only for photon addition, the region of positive  $\mathcal{D}_V^{\text{NG}}$  overlaps with the corresponding region of high success probability. Therefore, it can be concluded that out of all the non-Gaussian operations considered, only photon addition offers an advantage while taking

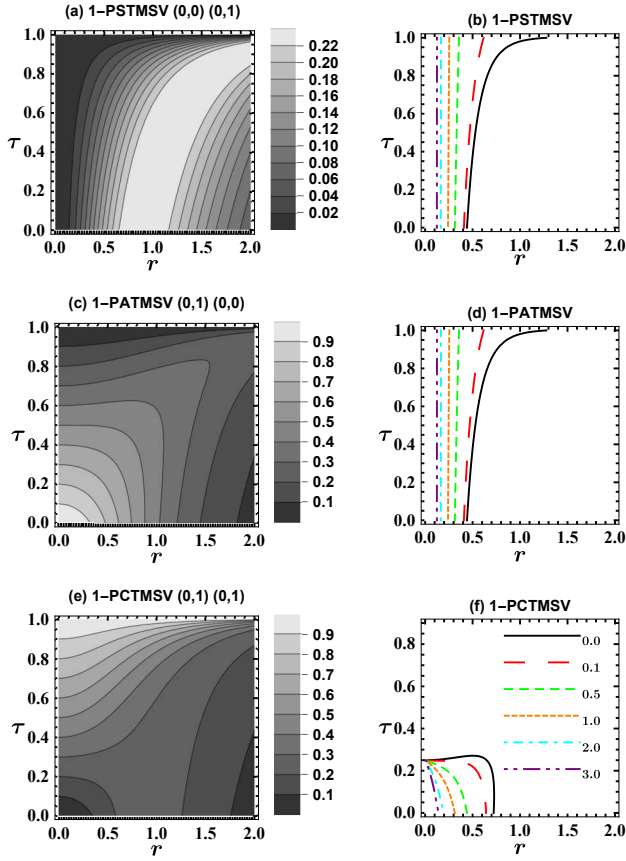


FIG. 7. Left panels show the success probability as a function of the transmissivity  $\tau$  and squeezing parameter  $\lambda$ . Right panels show the curves of fixed  $\mathcal{D}_V^{\text{NG}}$ , the difference of  $\Delta\phi$  between TMSV and NGTMSV states, as a function of  $\tau$  and  $\lambda$ . We have considered NGTMSV states generated by performing non-Gaussian operations on one of the modes of the TMSV state, and the corresponding values of the parameters  $(m_1, n_1)(m_2, n_2)$  have been shown. The legend on the right panel shows the plotted values of  $\mathcal{D}_V^{\text{NG}}$ . The phase,  $\phi$ , is taken to be 0.01. Both the axes are dimensionless.

the probabilistic nature of these operations into account. Reference [38] provides a detailed discussion of these results.

We now proceed to analyze the advantages rendered by the NGTMST states as compared to the TMST state. As shown in Fig. 7, we plot the success probability for various non-Gaussian operations in the left panel of Fig. 8, whereas the right panel show the plot for different fixed values of corresponding  $\mathcal{D}_T^{\text{NG}}$  ( $= 0, 1, 5, 20, 50, 100$ ) as a function of the transmissivity  $\tau$  and squeezing parameter  $r$ . There is a considerable enhancement in the magnitude of  $\mathcal{D}_T^{\text{NG}}$  in comparison to  $\mathcal{D}_V^{\text{NG}}$ . This signifies the fact that incremental advantage of performing non-Gaussian operations on the TMST state is much more as compared to that of performing these operations on the TMSV state.

On careful comparison of the left panels of Figs. 7 and 8, we observe that the maximum achievable success prob-

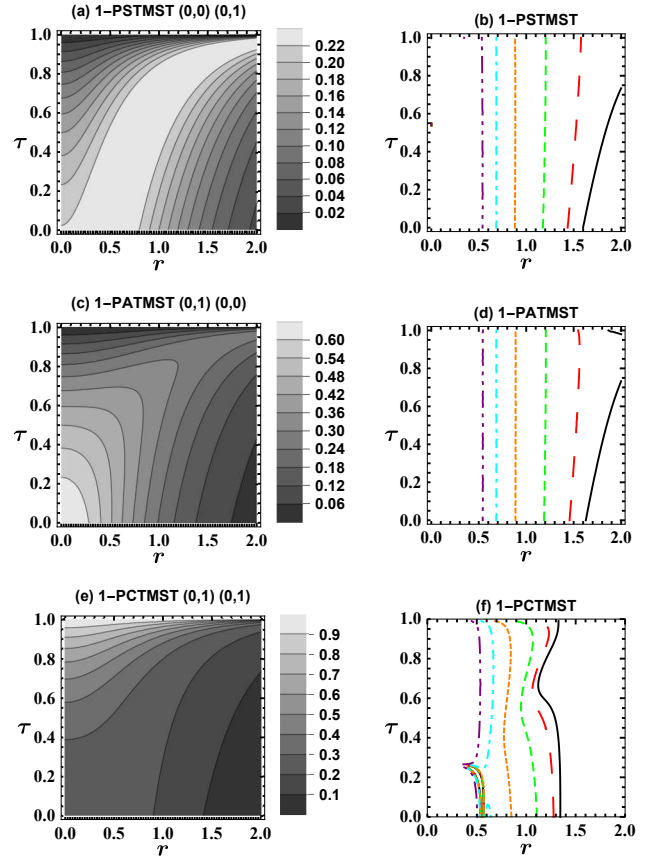


FIG. 8. Left panels show the success probability as a function of the transmissivity  $\tau$  and squeezing parameter  $\lambda$ . Right panels show the curves of fixed  $\mathcal{D}_T^{\text{NG}}$ , the difference of  $\Delta\phi$  between TMST and NGTMST states, as a function of  $\tau$  and  $r$ . We have considered NGTMST states generated by performing non-Gaussian operations on one of the modes of the TMST state, and the corresponding values of the parameters  $(m_1, n_1)(m_2, n_2)$  have been shown. The phase,  $\phi$ , is taken to be 0.01. Solid black, large dashed red, dashed green, dotted orange, dot dashed cyan, and double dot dashed purple curves represent  $\mathcal{D}_T^{\text{NG}}$  ( $= 0, 1, 5, 20, 50, 100$ ), respectively. Both the axes are dimensionless.

ability for PS and PC operations on the TMST state is approximately the same as on the TMSV state, whereas it decreases considerably for PA operation. Similarly, a careful comparison of the right panels reveals that the region of positive  $\mathcal{D}_T^{\text{NG}}$  in  $r$  and  $\tau$  space increases for all three non-Gaussian operations. While for PC operation, this change is due to an increase in the allowed values of both parameters  $r$  and  $\tau$ , for PA and PS operations, this is not the case as there is no scope for increment in  $\tau$  and only the allowed range of  $r$  is increased.

Taking the success probability considerations into account, we observe that only for photon catalysis, the region of positive  $\mathcal{D}_T^{\text{NG}}$  overlaps with the corresponding region of high success probability (large  $\tau$  regime). Therefore, photon catalysis offers maximum advantage while taking the probabilistic nature of non-Gaussian opera-



tions into account.

## V. CONCLUSION

In this article, we showed that performing non-Gaussian operations on TMST states enhances the phase sensitivity in parity detection based MZI. To this end, we derived a unified Wigner distribution function describing PSTMST, PATMST, and PCTMST states altogether. We utilize this function to obtain a single phase sensitivity expression for all three cases mentioned above. By appropriately changing the number of input and detected photon, we can perform PS, PA and PC operations. The Wigner function and the phase sensitivity depend on the initial squeezing of the TMST state, the average number of photons in the thermal state, the transmissivity of the beam splitter used in the implementation of the non-Gaussian operations, and the magnitude of the unknown phase introduced. A careful analysis involving the probabilistic nature of non-Gaussian operations reveals the photon catalysis operation as the most optimal non-Gaussian operation. These optimal conditions are achieved while working in a high transmissivity regime.

It is clear that the results of this study will be of significant relevance for any future phase estimation experiments involving TMST states. Recent experiments implementing PS operations on thermal states signal that our proposal could be implemented in lab [64]. Further, the derived Wigner function will be of great use in the state characterization via quantifying nonclassicality [65], entanglement [66], non-Gaussianity [67, 68], and nonlocality [69]. As mentioned earlier, we overcame the calculational challenges involved in dealing with non-Gaussian operations on TMST state by following phase space formalism instead of the traditional operator method. The phase space method utilized in this work can be useful in circumventing calculations challenges in various other problems as well, for instance, quantum teleportation via PCTMST states, a problem posed in Ref. [54]. While the scope of this paper is limited to exploring the advantages of performing non-Gaussian operation on a single mode of the TMST state, the effects of performing these non-Gaussian operations on both modes remain to be investigated.

## ACKNOWLEDGEMENT

This is the third article in a publication series written in the celebration of the completion of 15 years of IISER Mohali. C.K. acknowledges the financial support from **DST/ICPS/QuST/Theme-1/2019/General** Project number Q-68.

## Appendix A: Coefficients appearing in the Wigner function, probability and average of parity operator

The coefficients  $a_i$  appearing in Eq. (20) are given as

$$\begin{aligned} a_0 &= \pi^2 k (2k\mu^2 T + \Lambda r^2) \mu^{-2}, \\ a_1 &= kr^2 (2k\mu^2 + \Lambda) b_0^{-1}, \\ a_2 &= (2b_1 (q_1 - ip_1) + b_2 (q_2 + ip_2)) b_0^{-1}, \\ a_3 &= - (2b_1 (q_1 + ip_1) - ib_2 (p_2 + iq_2)) b_0^{-1}, \\ a_4 &= - kr^2 (2k\mu^2 - \Lambda) b_0^{-1}, \\ a_5 &= (2b_3 (q_1 - ip_1) + b_4 (q_2 + ip_2)) b_0^{-1}, \\ a_6 &= - (2b_3 (q_1 + ip_1) - ib_4 (p_2 + iq_2)) b_0^{-1}, \\ a_7 &= 4k^2 \mu^2 t b_0^{-1}, \end{aligned} \quad (\text{A1})$$

where  $\mu = \sqrt{1 - \lambda^2}$ ,  $t = \sqrt{\tau}$ ,  $r = \sqrt{1 - \tau}$ ,  $T = (1 + t^2)$ ,  $\Lambda = (1 + \lambda^2)$  and

$$\begin{aligned} b_0 &= -2k (2k\mu^2 T + \Lambda r^2), \\ b_1 &= 2k\lambda r t, \\ b_2 &= -kr (2k\mu^2 + \Lambda), \\ b_3 &= 2k\lambda r, \\ b_4 &= krt (2k\mu^2 - \Lambda). \end{aligned} \quad (\text{A2})$$

Further the matrix  $M_1$  appearing in Eq. (20) is given as

$$M_1 = \frac{1}{b_0} \begin{pmatrix} c_1 & 0 & c_2 & 0 \\ 0 & c_1 & 0 & -c_2 \\ c_2 & 0 & c_3 & 0 \\ 0 & -c_2 & 0 & c_3 \end{pmatrix}, \quad (\text{A3})$$

where

$$\begin{aligned} c_1 &= k\Lambda T + \mu^2 r^2, \\ c_2 &= -4k\lambda t, \\ c_3 &= k\Lambda T + 2k^2 \mu^2 r^2. \end{aligned} \quad (\text{A4})$$

The explicit form of matrix  $M_2$  appearing in Eq. (23) is given as

$$M_2 = \frac{1}{d_4} \begin{pmatrix} 0 & d_1 & 0 & d_2 \\ d_1 & 0 & d_2 & 0 \\ 0 & d_2 & 0 & d_3 \\ d_2 & 0 & d_3 & 0 \end{pmatrix}, \quad (\text{A5})$$

where

$$\begin{aligned} d_0 &= \frac{2\mu^2}{2k\Lambda r^2 + \mu^2 T}, \\ d_1 &= -r^2 (\mu^2 + 2k\Lambda), \\ d_2 &= -2\mu^2 t, \\ d_3 &= r^2 (\mu^2 - 2k\Lambda), \\ d_4 &= 8k\Lambda r^2 - 2\mu^2 T. \end{aligned} \quad (\text{A6})$$

The explicit form of matrix  $M_3$  appearing in Eq. (31) is given as

$$M_3 = \frac{1}{e_7} \begin{pmatrix} e_1 & e_2 & e_3 & e_4 \\ e_2 & e_1 & e_4 & e_3 \\ e_3 & e_4 & e_5 & e_6 \\ e_4 & e_3 & e_6 & e_5 \end{pmatrix}, \quad (\text{A7})$$

where

$$\begin{aligned} e_0 &= 8\mu^2 e_7^{-1/2}, \\ e_1 &= 8k\lambda r^2 t (s_2 f_4 - 2s_1 f_1 \mu^2), \\ e_2 &= f_6 r^2 (f_1 \mu^2 - c_1 f_4), \\ e_3 &= 8k\lambda r^2 s_1 (4k\Lambda r^2 - f_3 \mu^2 T), \\ e_4 &= -8kt [\Lambda \mu^2 r^2 (c_1 f_1 + f_2) + 4kT(\Lambda^2 - 4\lambda^2 s_1^2)], \\ e_5 &= 8k\lambda r^2 t (s_2 f_5 - 2s_1 f_1 \mu^2), \\ e_6 &= f_6 r^2 (f_1 \mu^2 - c_1 f_5), \\ e_7 &= 4 [(4k\Lambda T - f_3 \mu^2 r^2)^2 - (16k\lambda s_1 t)^2], \end{aligned} \quad (\text{A8})$$

where  $c_1 = \cos \phi$ ,  $s_1 = \sin \phi$ ,  $c_2 = \cos(2\phi)$ , and  $s_2 = \sin(2\phi)$  and

$$\begin{aligned} f_1 &= 4k^2 - 1, & f_4 &= f_2 \mu^2 + 4k\Lambda, \\ f_2 &= 4k^2 + 1, & f_5 &= f_2 \mu^2 - 4k\Lambda, \\ f_3 &= c_1 f_1 - f_2, & f_6 &= f_4 \mu^2 r^2 - 4k\Lambda T. \end{aligned} \quad (\text{A9})$$

- 
- [1] J. P. Dowling, Quantum optical metrology – the low-down on high-n00n states, *Contemporary Physics* **49**, 125 (2008).
- [2] V. Giovannetti, S. Lloyd, and L. Maccone, Advances in quantum metrology, *Nature Photonics* **5**, 222 (2011).
- [3] C. M. Caves, Quantum-mechanical noise in an interferometer, *Phys. Rev. D* **23**, 1693 (1981).
- [4] V. Giovannetti, S. Lloyd, and L. Maccone, Quantum-enhanced measurements: Beating the standard quantum limit, *Science* **306**, 1330 (2004).
- [5] H. F. Hofmann and T. Ono, High-photon-number path entanglement in the interference of spontaneously down-converted photon pairs with coherent laser light, *Phys. Rev. A* **76**, 031806 (2007).
- [6] P. M. Anisimov, G. M. Raterman, A. Chiruvelli, W. N. Plick, S. D. Huver, H. Lee, and J. P. Dowling, Quantum metrology with two-mode squeezed vacuum: Parity detection beats the heisenberg limit, *Phys. Rev. Lett.* **104**, 103602 (2010).
- [7] H. Kwon, K. C. Tan, T. Volkoff, and H. Jeong, Nonclassicality as a quantifiable resource for quantum metrology, *Phys. Rev. Lett.* **122**, 040503 (2019).
- [8] C. C. Gerry, Heisenberg-limit interferometry with four-wave mixers operating in a nonlinear regime, *Phys. Rev. A* **61**, 043811 (2000).
- [9] C. C. Gerry and R. A. Campos, Generation of maximally entangled photonic states with a quantum-optical fredkin gate, *Phys. Rev. A* **64**, 063814 (2001).
- [10] C. C. Gerry and A. Benmoussa, Heisenberg-limited interferometry and photolithography with nonlinear four-wave mixing, *Phys. Rev. A* **65**, 033822 (2002).
- [11] R. A. Campos, C. C. Gerry, and A. Benmoussa, Optical interferometry at the heisenberg limit with twin fock states and parity measurements, *Phys. Rev. A* **68**, 023810 (2003).
- [12] C. C. Gerry and J. Mimih, Heisenberg-limited interferometry with pair coherent states and parity measurements, *Phys. Rev. A* **82**, 013831 (2010).
- [13] C. C. Gerry and J. Mimih, The parity operator in quantum optical metrology, *Contemporary Physics* **51**, 497 (2010).
- [14] J. Joo, W. J. Munro, and T. P. Spiller, Quantum metrology with entangled coherent states, *Phys. Rev. Lett.* **107**, 083601 (2011).
- [15] K. P. Seshadreesan, P. M. Anisimov, H. Lee, and J. P. Dowling, Parity detection achieves the heisenberg limit in interferometry with coherent mixed with squeezed vacuum light, *New Journal of Physics* **13**, 083026 (2011).
- [16] W. N. Plick, P. M. Anisimov, J. P. Dowling, H. Lee, and G. S. Agarwal, Parity detection in quantum optical metrology without number-resolving detectors, *New Journal of Physics* **12**, 113025 (2010).
- [17] A. Chiruvelli and H. Lee, Parity measurements in quantum optical metrology, *Journal of Modern Optics* **58**, 945 (2011).
- [18] K. P. Seshadreesan, S. Kim, J. P. Dowling, and H. Lee, Phase estimation at the quantum cramer-rao bound via parity detection, *Phys. Rev. A* **87**, 043833 (2013).
- [19] J. Sahota and D. F. V. James, Quantum-enhanced phase estimation with an amplified bell state, *Phys. Rev. A* **88**, 063820 (2013).
- [20] X.-X. Zhang, Y.-X. Yang, and X.-B. Wang, Lossy quantum-optical metrology with squeezed states, *Phys. Rev. A* **88**, 013838 (2013).
- [21] H. Vahlbruch, M. Mehmet, K. Danzmann, and R. Schnabel, Detection of 15 db squeezed states of light and their application for the absolute calibration of photoelectric quantum efficiency, *Phys. Rev. Lett.* **117**, 110801 (2016).
- [22] P. Huang, G. He, J. Fang, and G. Zeng, Performance improvement of continuous-variable quantum key distri-

- bution via photon subtraction, *Phys. Rev. A* **87**, 012317 (2013).
- [23] H.-X. Ma, P. Huang, D.-Y. Bai, S.-Y. Wang, W.-S. Bao, and G.-H. Zeng, Continuous-variable measurement-device-independent quantum key distribution with photon subtraction, *Phys. Rev. A* **97**, 042329 (2018).
- [24] Y. Guo, W. Ye, H. Zhong, and Q. Liao, Continuous-variable quantum key distribution with non-gaussian quantum catalysis, *Phys. Rev. A* **99**, 032327 (2019).
- [25] W. Ye, H. Zhong, Q. Liao, D. Huang, L. Hu, and Y. Guo, Improvement of self-referenced continuous-variable quantum key distribution with quantum photon catalysis, *Opt. Express* **27**, 17186 (2019).
- [26] C. Kumar, J. Singh, S. Bose, and Arvind, Coherence-assisted non-gaussian measurement-device-independent quantum key distribution, *Phys. Rev. A* **100**, 052329 (2019).
- [27] L. Hu, M. Al-amri, Z. Liao, and M. S. Zubairy, Continuous-variable quantum key distribution with non-gaussian operations, *Phys. Rev. A* **102**, 012608 (2020).
- [28] T. Opatrný, G. Kurizki, and D.-G. Welsch, Improvement on teleportation of continuous variables by photon subtraction via conditional measurement, *Phys. Rev. A* **61**, 032302 (2000).
- [29] Y. Yang and F.-L. Li, Entanglement properties of non-gaussian resources generated via photon subtraction and addition and continuous-variable quantum-teleportation improvement, *Phys. Rev. A* **80**, 022315 (2009).
- [30] X.-x. Xu, Enhancing quantum entanglement and quantum teleportation for two-mode squeezed vacuum state by local quantum-optical catalysis, *Phys. Rev. A* **92**, 012318 (2015).
- [31] L. Hu, Z. Liao, and M. S. Zubairy, Continuous-variable entanglement via multiphoton catalysis, *Phys. Rev. A* **95**, 012310 (2017).
- [32] S. Wang, L.-L. Hou, X.-F. Chen, and X.-F. Xu, Continuous-variable quantum teleportation with non-gaussian entangled states generated via multiple-photon subtraction and addition, *Phys. Rev. A* **91**, 063832 (2015).
- [33] R. Birrittella, J. Mimih, and C. C. Gerry, Multiphoton quantum interference at a beam splitter and the approach to heisenberg-limited interferometry, *Phys. Rev. A* **86**, 063828 (2012).
- [34] R. Carranza and C. C. Gerry, Photon-subtracted two-mode squeezed vacuum states and applications to quantum optical interferometry, *J. Opt. Soc. Am. B* **29**, 2581 (2012).
- [35] D. Braun, P. Jian, O. Pinel, and N. Treps, Precision measurements with photon-subtracted or photon-added gaussian states, *Phys. Rev. A* **90**, 013821 (2014).
- [36] Y. Ouyang, S. Wang, and L. Zhang, Quantum optical interferometry via the photon-added two-mode squeezed vacuum states, *J. Opt. Soc. Am. B* **33**, 1373 (2016).
- [37] H. Zhang, W. Ye, C. Wei, Y. Xia, S. Chang, Z. Liao, and L. Hu, Improved phase sensitivity in a quantum optical interferometer based on multiphoton catalytic two-mode squeezed vacuum states, *Phys. Rev. A* **103**, 013705 (2021).
- [38] C. Kumar, Rishabh, and S. Arora, Realistic non-gaussian-operation scheme in parity-detection-based mach-zehnder quantum interferometry, *Phys. Rev. A* **105**, 052437 (2022).
- [39] R. H. BROWN and R. Q. TWISS, Correlation between photons in two coherent beams of light, *Nature* **177**, 27 (1956).
- [40] M. V. Chekhova, S. P. Kulik, A. N. Penin, and P. A. Prudkovskii, Intensity interference in bragg scattering by acoustic waves with thermal statistics, *Phys. Rev. A* **54**, R4645 (1996).
- [41] A. Gatti, E. Brambilla, M. Bache, and L. A. Lugiato, Ghost imaging with thermal light: Comparing entanglement and classical correlation, *Phys. Rev. Lett.* **93**, 093602 (2004).
- [42] F. Ferri, D. Magatti, A. Gatti, M. Bache, E. Brambilla, and L. A. Lugiato, High-resolution ghost image and ghost diffraction experiments with thermal light, *Phys. Rev. Lett.* **94**, 183602 (2005).
- [43] A. Valencia, G. Scarcelli, M. D'Angelo, and Y. Shih, Two-photon imaging with thermal light, *Phys. Rev. Lett.* **94**, 063601 (2005).
- [44] S. Lloyd, Enhanced sensitivity of photodetection via quantum illumination, *Science* **321**, 1463 (2008).
- [45] H.-M. Li, X.-X. Xu, H.-C. Yuan, and Z. Wang, Quantum metrology with two-mode squeezed thermal state: Parity detection and phase sensitivity, *Chinese Physics B* **25**, 104203 (2016).
- [46] I. Mahboob, H. Okamoto, K. Onomitsu, and H. Yamaguchi, Two-mode thermal-noise squeezing in an electromechanical resonator, *Phys. Rev. Lett.* **113**, 167203 (2014).
- [47] M. Rashid, T. Tufarelli, J. Bateman, J. Vovrosh, D. Hempston, M. S. Kim, and H. Ulbricht, Experimental realization of a thermal squeezed state of levitated optomechanics, *Phys. Rev. Lett.* **117**, 273601 (2016).
- [48] S. Cialdi, C. Porto, D. Cipriani, S. Olivares, and M. G. A. Paris, Full quantum state reconstruction of symmetric two-mode squeezed thermal states via spectral homodyne detection and a state-balancing detector, *Phys. Rev. A* **93**, 043805 (2016).
- [49] I. Mahboob, H. Okamoto, and H. Yamaguchi, Enhanced visibility of two-mode thermal squeezed states via degenerate parametric amplification and resonance, *New Journal of Physics* **18**, 083009 (2016).
- [50] L.-y. Hu, X.-x. Xu, Z.-s. Wang, and X.-f. Xu, Photon-subtracted squeezed thermal state: Nonclassicality and decoherence, *Phys. Rev. A* **82**, 043842 (2010).
- [51] X. guo Meng, Z. Wang, H. yi Fan, J. suo Wang, and Z. shan Yang, Nonclassical properties of photon-added two-mode squeezed thermal states and their decoherence in the thermal channel, *J. Opt. Soc. Am. B* **29**, 1844 (2012).
- [52] L.-Y. Hu, F. Jia, and Z.-M. Zhang, Entanglement and nonclassicality of photon-added two-mode squeezed thermal state, *J. Opt. Soc. Am. B* **29**, 1456 (2012).
- [53] L.-Y. Hu and Z.-M. Zhang, Nonclassicality and decoherence of photon-added squeezed thermal state in thermal environment, *J. Opt. Soc. Am. B* **29**, 529 (2012).
- [54] X.-G. Meng, K.-C. Li, J.-S. Wang, X.-Y. Zhang, Z.-T. Zhang, Z.-S. Yang, and B.-L. Liang, Continuous-variable entanglement and wigner-function negativity via adding or subtracting photons, *Annalen der Physik* **532**, 1900585 (2020).
- [55] Y. I. Bogdanov, K. G. Katamadze, G. V. Avosopiants, L. V. Belinsky, N. A. Bogdanova, A. A. Kalinkin, and S. P. Kulik, Multiphoton subtracted thermal states: Description, preparation, and reconstruction, *Phys. Rev. A* **96**, 063803 (2017).

- [56] G. V. Avosopiants, B. I. Bantysh, K. G. Katamadze, N. A. Bogdanova, Y. I. Bogdanov, and S. P. Kulik, Statistical parameter estimation of multimode multiphoton-subtracted thermal states of light, *Phys. Rev. A* **104**, 013710 (2021).
- [57] T. J. Bartley and I. A. Walmsley, Directly comparing entanglement-enhancing non-gaussian operations, *New Journal of Physics* **17**, 023038 (2015).
- [58] H. yi Fan, Operator ordering in quantum optics theory and the development of dirac s symbolic method, *Journal of Optics B: Quantum and Semiclassical Optics* **5**, R147 (2003).
- [59] A. Royer, Wigner function as the expectation value of a parity operator, *Phys. Rev. A* **15**, 449 (1977).
- [60] C. Weedbrook, S. Pirandola, R. García-Patrón, N. J. Cerf, T. C. Ralph, J. H. Shapiro, and S. Lloyd, Gaussian quantum information, *Rev. Mod. Phys.* **84**, 621 (2012).
- [61] Arvind, B. Dutta, N. Mukunda, and R. Simon, The real symplectic groups in quantum mechanics and optics, *Pramana* **45**, 471 (1995).
- [62] B. Yurke, S. L. McCall, and J. R. Klauder,  $Su(2)$  and  $su(1,1)$  interferometers, *Phys. Rev. A* **33**, 4033 (1986).
- [63] R. J. Birrittella, P. M. Alsing, and C. C. Gerry, The parity operator: Applications in quantum metrology, *AVS Quantum Science* **3**, 014701 (2021).
- [64] Y. I. Bogdanov, K. G. Katamadze, G. V. Avosopiants, L. V. Belinsky, N. A. Bogdanova, A. A. Kalinkin, and S. P. Kulik, Multiphoton subtracted thermal states: Description, preparation, and reconstruction, *Phys. Rev. A* **96**, 063803 (2017).
- [65] W. Ge and M. S. Zubairy, Evaluating single-mode non-classicality, *Phys. Rev. A* **102**, 043703 (2020).
- [66] M. Allegra, P. Giorda, and M. G. A. Paris, Role of initial entanglement and non-gaussianity in the decoherence of photon-number entangled states evolving in a noisy channel, *Phys. Rev. Lett.* **105**, 100503 (2010).
- [67] J. S. Ivan, M. S. Kumar, and R. Simon, A measure of non-gaussianity for quantum states, *Quantum Information Processing* **11**, 853 (2012).
- [68] J. Park, J. Lee, K. Baek, and H. Nha, Quantifying non-gaussianity of a quantum state by the negative entropy of quadrature distributions, *Phys. Rev. A* **104**, 032415 (2021).
- [69] C. Kumar, G. Saxena, and Arvind, Continuous-variable clausen-horne bell-type inequality: A tool to unearth the nonlocality of continuous-variable quantum-optical systems, *Phys. Rev. A* **103**, 042224 (2021).